Effects of compatibility of deproteinized antler cancellous bone with various bioactive factors on their osteogenic potential

CrossMark

Xuehui Zhang [a,b,1], Mingming Xu [a,1], Lin Song [c], Yan Wei [a], Yuanhua Lin [b], Wentao Liu [d], Boon C. Heng [e], Hui Peng [a], Ying Wang [a], Xuliang Deng [a,f,*]

[a] Department of Geriatric Dentistry, Peking University School and Hospital of Stomatology, Beijing 100081, PR China
[b] State Key Laboratory of New Ceramics and Fine Processing, and Department of Materials Science and Engineering, Tsinghua University, Beijing 100084, PR China
[c] Department of Periodontics, School of Stomatology, Capital Medical University, Beijing 100050, PR China
[d] Key Laboratory of Zoonosis, Ministry of Education, Institute of Zoonosis, College of Veterinary Medicine, Jilin University, Changchun 130062, PR China
[e] Department of Biosystems Science & Engineering (D-BSSE) ETH-Zurich, Mattenstrasse 26, Basel 4058, Switzerland
[f] National Engineering Laboratory for Digital and Material Technology of Stomatology, Beijing 100081, PR China

ARTICLE INFO

ABSTRACT

Combinations of calcium phosphate scaffolds and bioactive factors are promising niche-mimetic solutions for repairing large-sized bone defects. However, the importance of compatibility between scaffolds and bioactive factors on their osteogenic outcomes has been largely ignored. This study aimed to investigate the compatibility of calcinated antler cancellous bone (CACB) scaffolds with various bioactive factors including icariin (ICA), velvet antler polypeptides (VAP) or recombinant human bone morphogenetic protein-2 (rhBMP-2) as well as their combinational osteogenic potential in vitro and in vivo. Scanning electron microscopy and fourier transform infrared spectroscopy confirmed the uniform distribution and chemical stability of the reagents on CABC. In vitro release profiles showed relative steady release of ICA from ICA/CACB, burst VAP release from VAP/CACB, and minimal rhBMP-2 release from rhBMP-2/CACB composites. When compared with VAP and rhBMP-2, incorporation of ICA within CACB resulted in most increased cell attachment, proliferation, alkaline phosphatase activity, osteogenic gene expression, and mineralization of rat bone marrow mesenchymal stem cells. In rabbit mandible critical-sized defects, the most extensive osteogenesis and neovascularization were observed in the ICA/CACB group. Differences between the VAP/CACB and rhBMP-2/CACB groups were not apparent. Interestingly, low pro-inflammatory (TNF-α, IL-6) and high anti-inflammatory (IL-10) mRNA levels were observed at scaffold implantation sites which were in close association with amount of new bone formation. These findings highlight that the compatibility between scaffolds and bioactive factors should been taken into account when considering the formula of optimized bone defect repair.

© 2013 Elsevier Ltd. All rights reserved.

1. Introduction

Autogenic bone graft implantation is the major treatment modality for large-sized bone deficiencies arising from various diseases, traumas and congenital defects, and is regarded as the clinical gold standard [1]. The therapeutic success of autografts is mainly attributed to their identical chemistry and architecture to the surrounding bone tissue, as well as the presence of necessary bioactive factors required for bone regeneration [2]. However, the limited availability and donor site morbidity associated with autografts restricts their extensive usage in the clinic [3]. These limitations have already led to the pursuit of alternatives including allografts, xenografts and synthetic bone substitutes [4]. To enhance their repair efficacy, bone graft substitutes are often combined with bioactive factors, as an attempt to replicate the osteogenic niche provided by autografts [5–7]. Generally, bioactive factors can be non-covalently incorporated into scaffolds by three approaches, including physical entrapment, physical adsorption and ionic complexation [8,9]. Direct physical adsorption of bioactive factors onto apatite matrix scaffold such as hydroxyapatite (HA) particles [10], tricalcium phosphate particles [11], and deproteinized cancellous bone [12] is the most feasible, efficient,

* Corresponding author. Department of Geriatric Dentistry, Peking University School and Hospital of Stomatology, Beijing 100081, PR China. Tel.: +86 10 82195637; fax: +86 10 82195581.
E-mail address: kqdengxuliang@bjmu.edu.cn (X. Deng).
[1] These authors contributed equally to this work.

and most commonly utilized method for clinical applications in bone defect repair. The retention and bioactivity maintenance of active factors on scaffolds could be affected by the physiochemical properties of employed materials and bioactive factors. On the one hand, bioactive factors adsorption are influenced by surface wettability, roughness, surface charge and functional groups of matrix scaffolds [13]. On the other hand, molecular weight and isoelectric point of bioactive factors contribute largely to their adsorption to matrix scaffolds [13]. Therefore, understanding the compatibility or interactions between scaffolds and bioactive factors will be imperative and fundamental for their combinational applications in bone defect repair. However, to date, not much attention has been paid to this issue and scientific data is especially lacking.

Various types of bioactive factors (growth factors or biomolecules) have been reported to possess osteogenic capacity [7,14–16]. Bone morphogenetic protein-2 (BMP-2) is one kind of biomacromolecules and it is the prototypical and most common growth factor utilized for bone tissue engineering [17,18], and is commercially available in its recombinant human form (rhBMP-2). Velvet antler polypeptides (VAP) are the main pharmacologically active component of velvet antler, an animal-derived product utilized in traditional Chinese medicine [19]. Their molecular weight is much lower than that of rhBMP-2. There are reports that VAP can improve osteoblast viability and accelerate fracture healing [20,21]. Icariin (ICA) is a small molecule compound, and is the major active constituent of the *Epimedium* family of herbs (commonly known as horny goat weed), which has been extensively researched in the field of regenerative medicine. Previous studies have shown that ICA can promote osteoblast differentiation [22–24] and inhibit osteoclast formation [25,26]. It could accelerate bone regeneration when loaded into calcium phosphate cement scaffold [7], β-tricalcium phosphate (β-TCP) ceramic [27], and poly lactic-co-glycolic acid/tricalcium phosphate (PLGA/TCP) porous scaffold [28]. Although the osteogenic performance of above-mentioned three bioactive factors with different molecular weight, different reactive domains, and different sources including human, animal, and herb have been studied, their compatibility with matrix scaffolds especially calcium phosphate (CaP) scaffolds has been largely ignored.

Deproteinized inorganic xenogenic bone grafts, as a type of CaP scaffolds have been extensively utilized for bone augmentation because they possess favorable biocompatibility and osteoconductivity due to their close similarity in mineral composition, physical properties, and interconnecting pore structure to human cancellous bone [29–31]. In our previous study, we proposed a source of inorganic xenogenic bone: calcinated antler cancellous bone (CACB) [32]. The impressive osteoconduction and neovascularization efficacy of CACB is considered attributed to its porous structure and apatite crystal morphology, which are similar to human bone [32]. As the result of its stability in compositions and architecture, CACB might be used as CaP based scaffold to study the compatibility between bioactive factors and apatite scaffold in osteogenic performance.

Given the varying characteristics and different species origin of ICA, VAP and rhBMP-2, and the osteoconductive properties of CACB, the purpose of this study was to evaluate the utility of CACB as a vehicle for these three bioactive factors, and to investigate and compare the effects of their compatibility on osteogenic outcomes. The loading and release characteristics of these bioactive factors, together with the interactive response of rat bone marrow mesenchymal stem cells (rBMSCs) to these composites in term of adhesion, proliferation, osteogenic differentiation and mineralization were investigated *in vitro*. Furthermore, their efficacy in promoting *in situ* bone regeneration, neovascularization and modulation of inflammatory responses in a rabbit mandibular critical-sized defect model was also evaluated.

2. Materials and methods

2.1. Materials

Naturally shed antlers from adult male sika deer (*Cervus nippon*) were purchased from Jilin Wilderness Trading Company (Changchun, China). Human cancellous bone (gamma irradiated and freeze-dried vertebral bone; Batch No. 3460285/2009) was kindly provided by Ao Rui Biological Material Co., Ltd. (Shanxi, China). Sodium hydroxide, chloroform methanol and hydrogen peroxide were obtained from Sigma–Aldrich Inc. (St. Louis, MO, USA). ICA (molecular formula, $C_{33}H_{40}O_{15}$; molecular weight, 676.67 Da) was purchased from the National Institute for the Control of Pharmaceuticals and Biological Products (Beijing, China). VAP (molecular weight, 3.2 kDa) was provided as a gift by Jilin Natural Medicine Company (Jilin, China). rhBMP-2 was purchased from Sigma Aldrich Inc. (St. Louis, MO). rBMSCs were purchased from Cyagen Biosciences Inc. (Guangzhou, China).

2.2. Preparation of bioactive factors for loading onto CACB

The cancellous portions of naturally shed fresh antlers were obtained by removing the cortex. To eliminate the organic components of the bone blocks, chemical treatments and high temperature calcination were carried out, as described in our previous study [32]. Briefly, the cancellous bone blocks were immersed in 2% (w/v) sodium hydroxide for 12 h, and then in 30% hydrogen peroxide for 24 h; followed by washing under flowing tap water. The pieces were immersed in a 3:1 mixture of chloroform and methanol for 1 h and dried at 70 °C for 24 h. The dried pieces were then sintered at 800 °C over a period of 6 h and maintained at that temperature for 3 h in a tube-type furnace to obtain CACB. The bone blocks were milled and sieved to obtain granules with diameters ranging between 1.0 and 2.0 mm, as shown in Fig. 1B-a.

To load bioactive factors onto CACB, 0.25 g of CACB granules were soaked in 2 ml of sterile deionized water containing either 8.0 μg ICA at a concentration of 4.0 μg/ml ($≈ 6.0 × 10^{-6}$ M), 200 μg VAP at a concentration of 100 μg/ml, or 200 ng BMP-2 at a concentration of 100 ng/ml. These concentrations were based on experimental protocols of previous studies [20,33,34]. The composites obtained were then freeze dried in an ice condenser at −55 °C and negative pressure of 500 Pa.

2.3. Characterization

The surface morphology of pure CACB was examined by microcomputed tomography scanning (μ-CT; Skyscan 1072, Aartselaar, Belgium). The phase composition of CACB and calcinated human bone was analyzed by powder X-ray diffraction spectroscopy (XRD, Rigaku D/max 2500 VB2+/PC, Japan). Scanning electron microscopy (SEM; S-3000N, Hitachi, Japan) was used to observe the microstructure of the samples and distribution of bioactive factors on CACB scaffolds. Fourier transform infrared spectroscopy (FTIR; Avatar 360, Nicolet Co., USA) was used to evaluate the infrared absorption spectra of ICA, VAP, BMP-2 and CACB in the 4000–400 cm^{-1} range.

2.4. In vitro release assay

Composites were immersed in 5 ml of phosphate-buffered saline (PBS) solution (pH 7.4) and gently shaken at 100 rpm at 37 °C. At predetermined time points of 0.5 h, 1 h, 2 h, 3 h, 6 h, 12 h, and 1, 2, 4, 7, 10, and 14 days, fresh medium was replaced. The amount of released ICA compound was determined using a UV–vis spectrophotometer (DU-530, Beckman Coulter™, USA) at 270 nm as described the previous studies [27]. The amount of released VAP as a polypeptide mixture was quantified as the total protein concentration using a Micro-BCA protein assay kit (Pierce, Rockford, IL). The amount of released rhBMP-2 was evaluated with a BMP-2 Immunoassay kit (R&D Quantikine #DBP200, USA) using a microplate reader (Bio-Rad, Hercules, CA, USA). The enzyme-linked immunosorbent assay method described by Chen et al. was adopted for quantification [35].

2.5. In vitro bioactivity assay

2.5.1. Attachment and proliferation of rBMSCs
rBMSCs ($5 × 10^5$ cells/well) were seeded onto experimental scaffolds in 24-well plates, and incubated *in vitro* at 37 °C in a humidified atmosphere with 5% CO$_2$. After 1 day of culture, the samples were fixed in 2.5% glutaraldehyde and serially dehydrated with an increasing ethanol gradient, air-dried in a hood and sputtered with gold prior to imaging under SEM (S-3000N, Hitachi, Japan) at 20 kV. The cell spreading areas were measured using Image J software (National Institutes of Health, Bethesda, MD, USA) employing a random sampling method. Cell proliferation was assayed using a CCK-8 kit (Dojindo, Japan) at 1, 3, 5 and 7 days of culture, with the absorbance being read at a wavelength of 450 nm, using an enzyme linked immunosorbent assay reader (Bio-Rad, Hercules, CA, USA).
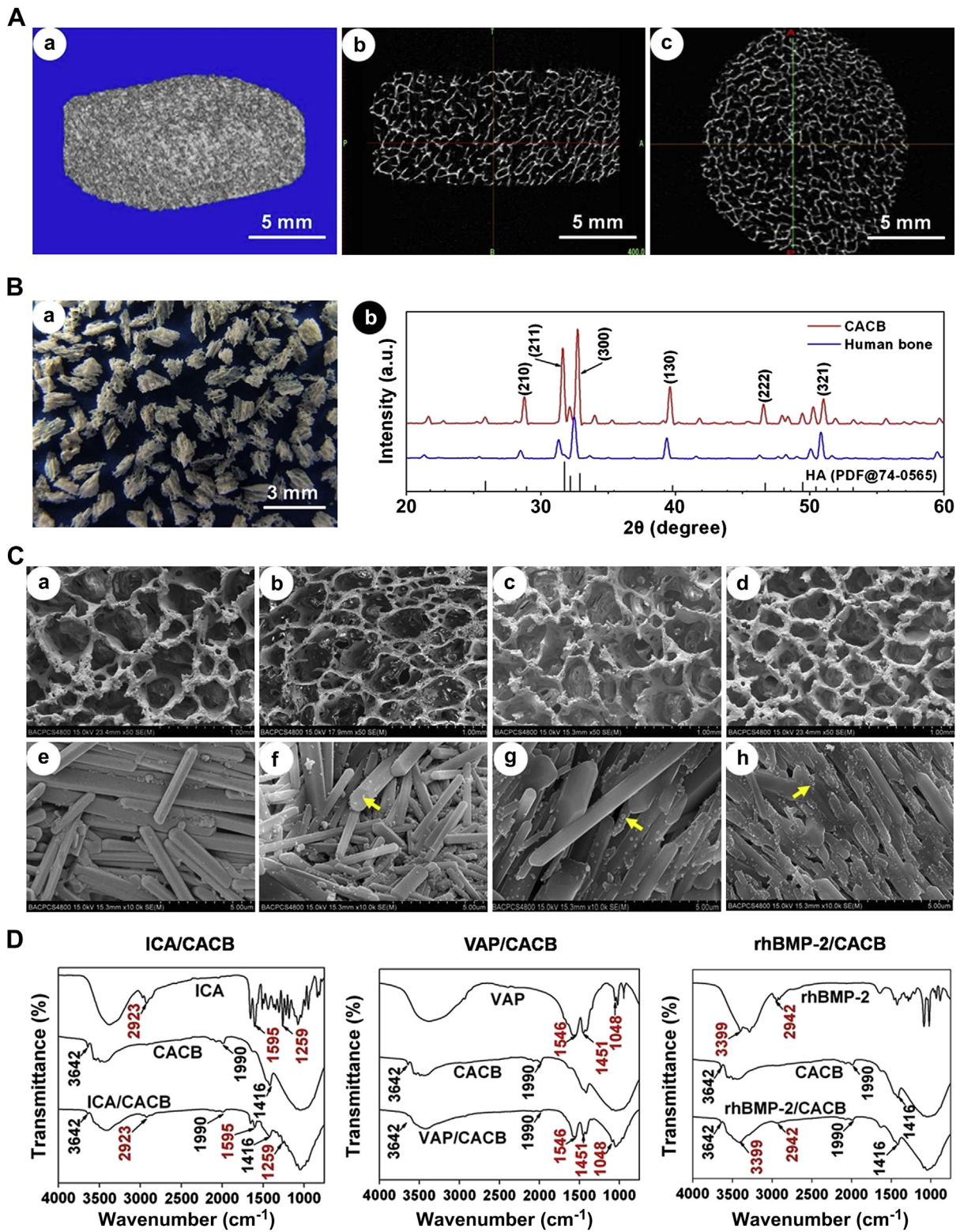
Fig. 1. Characterization of CACB and bioactive factor-loaded CACB scaffolds. (A) μ-CT images of (a) three-dimensional and (b, c) two-dimensional reconstruction of CACB cube. (B) The macroscopic image (a) and XRD patterns (b) of CACB scaffolds. (C) SEM images of CACB surface before and after loading of bioactive factors. (a, e) pure CACB; (b, f) ICA/CACB; (c, g) VAP/CACB; and (d, h) rhBMP-2/CACB. Yellow arrows denote the bioactive molecular particulates. The lower images are the enlargement of specific regions of the upper images. (D) FT-IR spectroscopy of CACB loaded with different bioactive factors. (For interpretation of the references to color in this figure legend, the reader is referred to the web version of this article.)

2.5.2. Alkaline phosphatase (ALP) activity assay

rBMSCs/scaffolds ($n = 6$) were continually cultured in wells. At 4 and 10 days, the ALP activity of the adherent cells was assessed using an Alkaline Phosphatase Assay Kit (Abcam, Cambridge, MA) according to the manufacturer's instructions. The absorbance was measured at a wavelength of 405 nm, and values of ALP activity were read off a standard curve based on standard samples provided by the Kit itself.

2.5.3. Quantitative real-time PCR analysis

Total RNA was extracted from each sample using TRIZOL reagent (Gibco-BRL, Gaithersburg, MD) following the manufacturer's instructions. The concentrations of the isolated RNA were determined spectrophotometrically at 260 nm using a NanoDrop ND-2000 Spectrophotometer (Thermo Fisher Scientific, Wilmington, DE). The RNA was then reverse transcribed to generate cDNA using the Reverse Transcription System (Promega, Madison, WI). Real-time RT-PCR was performed by using SYBR Green Detection System with an ABI PRISM 7500 Real-Time PCR System (Applied Biosystems, Foster City, CA). All reactions were carried out in triplicates. The primer sequences of osteogenic genes including ALP, runt-related transcription factor 2 (RUNX-2), collagen type I (COL 1A1) and osteocalcin (OCN) are listed in Table 1.

2.5.4. Alizarin Red S staining for mineralization

Alizarin Red S staining had previously been used to visualize calcium-rich deposits of cells in culture [36]. To evaluate the bioactivity of released growth factors, CACB scaffolds loaded with ICA, VAP or rhBMP-2 were immersed in standard DMEM containing 0.25 mM ascorbic acid, 10 mM β-glycerophosphate and 10 nM dexamethasone. After 2 days, the culture medium with eluted bioactive factors was harvested as a conditioned media for treatment of a pre-prepared rBMSCs monolayer pre-seeded at a density of 10^5 cells within 6-well plates ($n = 3$). On day 21, the cells grown in the conditioned media were fixed in 4% paraformaldehyde for 15 min, and then stained in 1% (w/v) Alizarin Red S (pH 4.1–4.5, Sigma Aldrich) for 30 min at room temperature. After washing in distilled water thrice, images were taken. In the quantitative analysis, the Alizarin Red stain on the specimen was dissolved in 10% cetylpyridinium chloride (Sigma Aldrich) in 10 mM sodium phosphate to measure the absorbance values at 620 nm.

2.6. In vivo osteogenesis evaluation

2.6.1. Animals and surgical procedures

A total of twenty-four male rabbits (New Zealand White, about 3.0 kg of weight) were used in this study. The experimental protocol was approved by the Animal Care and Use Committee of Peking University. Rabbits were divided randomly into five groups: (1) 12 defects for implantation of ICA/CACB; (2) 12 defects for implantation of VAP/CACB; (3) 12 defects for implantation of rhBMP-2/CACB; (4) 6 defects for implantation of pure CACB without bioactive factors; (5) 6 defects were left untreated as blank controls. Both sides of the mandible were utilized for creating bone defects.

Circular critical-sized defects, 8-mm in diameter were made in the mandible body as described in our previous study [32], and 0.25 g of pure CACB, ICA/CACB, VAP/CACB, or rhBMP-2/CACB composite granules were implanted into the defects. Rabbits from each group were sacrificed by lethal intravenous administration of sodium pentobarbital at 4 and 12 weeks post-implantation.

2.6.2. Microcomputed tomography (μ-CT) scanning evaluation

At 4 and 12 weeks post-implantation, mandibles were harvested intact, and fixed in 4% paraformaldehyde for 24 h at 4 °C, and the specimens were examined using μ-CT scanning as previously described [32]. Files were reconstructed using a modified Feldkamp algorithm, which was created using a microtomographic analysis software (Tomo NT; Skyscan, Belgium). After three-dimensional (3D) visualization, bone morphometric analyses, including calculation of bone mineral density (BMD) and bone volume fraction (Bone volume/total volume, BV/TV) measurements, were carried out on the region of interest (ROI).

2.6.3. Histological analysis

Tissue processing and sectioning were carried out as previously described [32]. Briefly, tissue samples were fixed in 10% neutral buffered formalin for 7 days,

decalcified and dehydrated according to standard protocols, embedded in paraffin and sectioned at 5 μm thickness. H&E staining and Masson's trichrome staining were performed separately on tissue sections, according to the manufacturer's protocols, and images were captured under light microscope (CX21, Olympus, Japan).

2.6.4. Immunohistochemical analysis

Immunohistochemistry for COL I, OCN, and CD31 was performed as previously described [37,38]. Briefly, tissue slides were deparaffinized and rehydrated, then submerged in hydrogen peroxide to quench peroxidase activity. Before exposure to the primary antibody against COL I (ab90395, CA 1:100, Abcam) or OCN (ab13420, CA 1:100, Abcam), slides were incubated with 1% BSA to block nonspecific binding. After incubation with primary antibody overnight at 4 °C, HRP conjugated secondary antibody was applied to the slides for 1 h at room temperature. Finally, the diaminobenzidine (DAB; Beyotime, Jiangsu, China) kit was used to develop the color, followed by counterstaining with hematoxylin. Slides were observed under a light microscope (CX21, Olympus, Japan). COL I and OCN expression within the defect area was quantified using a web application software ImunoRatio [38,39].

The number of microvessels at the implantation site was determined by analyzing the sections immunostained with anti-CD31 antibodies (1:200; Abcam, Cambridge, MA). A vascular section was defined as a vessel with a recognizable lumen. Microhemorrhages were excluded in the vessel count. The evaluation was performed by three different individuals who were blinded to the sample treatment.

2.6.5. Quantitative real-time PCR analysis

Samples from each experimental group were collected. The periosteum was stripped off. These were then flash-frozen and grounded into powder under liquid nitrogen. Total RNA was extracted using the RNeasy Mini Kit (Qiagen, Valencia, CA, US) and the concentration was determined spectrophotometrically. Then, 1 μg of RNA was used to synthesize cDNA with the First Strand cDNA Synthesis Kit (GeneCopoeia Inc, USA) according to the manufacturer's instruction. Quantitative real-time PCR reactions were carried out and monitored with an ABI PRISM 7500 Real-Time PCR System (Applied Biosystems, Foster City, CA). The amplifications were performed in triplicates for each sample with the following PCR conditions 95 °C, 30 s for 1 cycle; 60 °C, 30 s and 72 °C, 30 s for 45 cycles. The primer sequences of osteogenic genes (COL 1A1, OCN), vasculogenic genes (vascular endothelial growth factor, VEGF) and inflammatory genes (TNF-α, IL-6 and IL-10) are listed in Table 2. The data was analyzed with the $2^{-\Delta\Delta CT}$ method [40]. The RT-PCR products were also analyzed by electrophoresis in 2.5% agarose gels stained with ethidium bromide.

2.7. Statistical analysis

All quantitative data were expressed as mean ± standard deviation (SD). Statistical analyses were performed using the SPSS 19.0 software (Chicago, IL). Statistical differences were determined using Student's t test for independent samples. Differences between groups of $^*p < 0.05$ were considered statistically significant and $^{**}p < 0.01$ was considered highly significant.

3. Results

3.1. Loading characteristics of bioactive factors onto CACB

Representative 2D and 3D reconstructed μ-CT images of pure CACB cube are shown in Fig. 1A. The well-interconnected and highly porous structure was observed consistently throughout the entire scaffold, even if the bone blocks was milled into particles (Fig. 1B-a). The XRD patterns demonstrated that the characteristic peaks of CACB corresponded to the main diffraction peaks of stoichiometric HA and that of calcinated human cancellous bone (Fig. 1B-b).

Table 1
Primers sequences utilized for real time RT-PCR in vitro study.

Target gene	Forward primer sequence (5′–3′)	Reverse primer sequence (5′–3′)
ALP	TCCCACGTTTTCACGTTT	GAGACGTTCTCCCGTTCAC
RUNX-2	AATGCCTCCGCTGTTATG	TTCTGTCTGTGCCTTCTTG
COL1A1	GGAGAGAGTGCCAACTCCAG	CCACCCCAGGGATAAAAACT
OCN	ATGAGGACCCTCTCTCTGCTCA	CTAGCTCGTCACAATTGGGGTT
GAPDH	CTGATGCCTCCATGTTTGTG	GGATGCAGGGATGATGTTCT

Table 2
Primer sequences utilized for real time RT-PCR in vivo study.

Target gene	Forward primer sequence (5′–3′)	Reverse primer sequence (5′–3′)
COL1A1	AGCGTGGCCTACCTGGATGAAGC	ATGGGCGCGATGTCGGTGATGG
OCN	GAAGCCCAGCGGTGCA	CACTACCTCGCTGCCCTCC
VEGF	TGCCCACCGAGGAGTTCA	GGCCCTGGTGAGGTTTGAT
TNF-α	TCCGTGAAAACAGAGCAGAA	GAGCAGAGGTTCGGTGATGT
IL-6	GCTTGAGGGTGGCTTCTTC	GCTTGAGGGTGGCTTCTTC
IL-10	CCTTTGGCAGGGTGAAGACT	ATGGCTGGACTGTGGTTCTC
GAPDH	CTGATGCCTCCATGTTTGTG	GGATGCAGGGATGATGTTCT

SEM images of CACB before and after the addition of bioactive factors are shown in Fig. 1C. Tiny bioactive factor particulates were observed to be uniformly distributed on the surfaces and innermost regions of the CACB scaffolds (arrow). FTIR spectrograms (Fig. 1D) displayed the characteristic peaks of ICA (2923, 1595 and 1259 cm^{-1}), VAP (1546, 1451 and 1048 cm^{-1}) and rhBMP-2 (3399 and 2942 cm^{-1}) in the ICA/CACB, VAP/CACB and rhBMP-2/CACB composites, which indicated that these bioactive factors had not undergone any chemical modifications while being incorporated within the composite scaffolds.

3.2. In vitro release profiles of bioactive factors

The release profiles of ICA, VAP, and rhBMP-2 from their corresponding composites are shown in Fig. 2. ICA/CACB displayed relative stable release of ICA, and the eluted amount was determined to be 54 ± 2.32% of the original load after 14 days. VAP/CACB showed a maximal burst release of VAP, and the total eluted amount was 86 ± 1.85% of the original load after 14 days. By contrast, only a small amount of rhBMP-2 was released from the rhBMP-2/CACB, and the total eluted amount did not exceed 20% of the original load after 14 days.

3.3. In vitro bioactivity of composites

3.3.1. Morphology of rBMSCs on bioactive factor-loaded CACBs
Fig. 3A showed that rBMSCs seeded on CACB composites loaded with bioactive factors, displayed more apparent cellular processes after 1 day of culture (Fig. 3A, b–d), as well as larger cell spreading area (Fig. 3B) compared to cells grown on pure CACB scaffolds without any bioactive factors. There was however no obvious differences in cell morphology among the three types of CACB composites loaded with different bioactive factors.

3.3.2. rBMSCs proliferation on bioactive factor-loaded CACBs
Fig. 3C showed the proliferation of rBMSCs cultured on various CACB composites loaded with different bioactive factors. Overall, there was no significant difference between pure CACB and the CACB/VAP composite during the entire culture period. By comparison, cell proliferation on ICA/CACB yielded the best results followed by rhBMP-2/CACB.
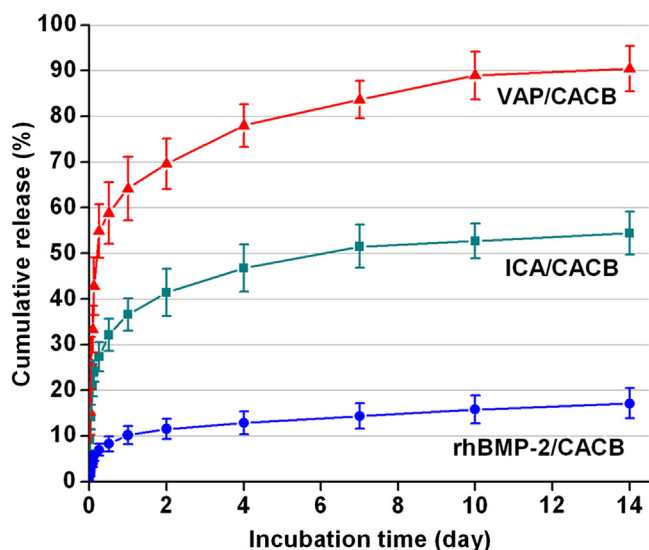
3.3.3. ALP activity of rBMSCs on bioactive factor-loaded CACBs
As seen in Fig. 3D, the ALP activity of rBMSCs seeded on ICA/CACB displayed the most enhancement, followed by rhBMP-2/CACB after 4 days of culture. This increase was maintained on day 10. There were no significant differences in ALP activity of rBMSCs seeded on VAP/CACB and pure CACB at either timepoint.

3.3.4. Osteogenic differentiation of rBMSCs
ALP, RUNX-2, COL 1A1 and OCN mRNA expression profiles at 4 and 10 days are shown in Fig. 3E. Compared to pure CACB scaffolds, all three types of CACB composites loaded with different bioactive factors promoted higher expression of selected osteogenic genes. ICA/CACB yielded the best results. Upon comparing VAP/CACB and rhBMP-2/CACB, there were observed to be significant differences in RUNX-2 and COL 1A1 expression but no apparent differences in ALP and OCN expression.

3.3.5. Mineralization of rBMSCs
Fig. 4 shows the mineralization of rBMSCs visualized by Alizarin Red S staining. ICA/CACB displayed the most intense staining, followed by rhBMP-2/CACB and VAP/CACB. The dissolution product of CACB apparently increased calcium deposits, but there was still observed to be less intense staining with CACB alone, as compared to VAP/CACB.
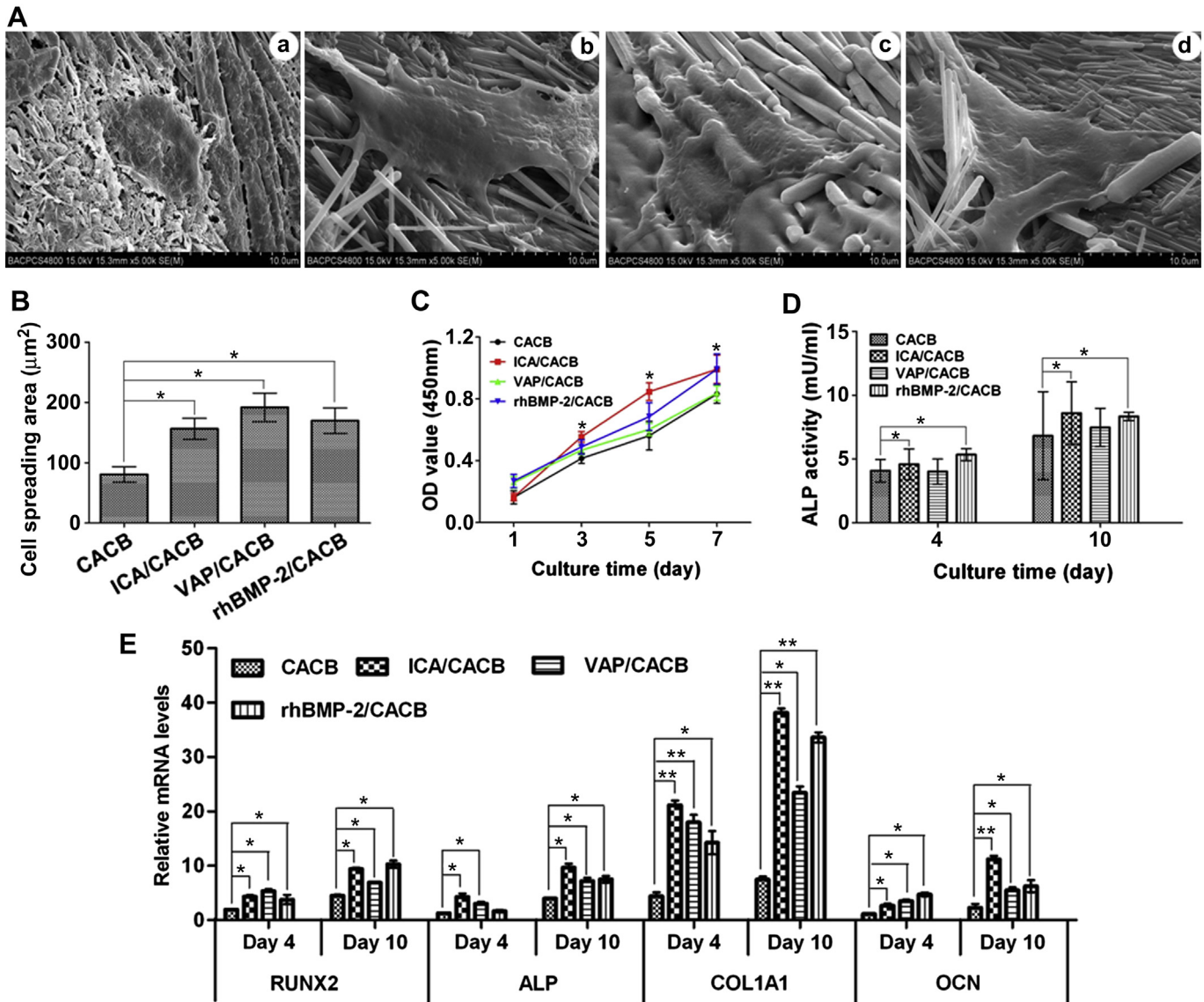
3.4. In vivo osteogenesis of composites

3.4.1. Quality and quantity of new bone formation
The representative 3D morphological images of repaired mandible defects obtained by μ-CT scanning are shown in Fig. 5A. Qualitatively, at 4 weeks post-implantation, substantial new bone formation was observed in all the scaffold-implanted groups. By 12 weeks, the regenerated bone tissue was flush with the surrounding host bone tissue for all treatment groups. The surface morphology of the healed defects, especially in the ICA/CACB group, closely resembled that of the surrounding normal bone (Fig. 5A-h). In the untreated group, the mandibular defect was left with an obvious introcession (Fig. 5A-f). The quantity of newly formed bone in the defect sites was calculated by morphometric analyses (Fig. 5B and C). The local BMD values closely corresponded to the BV/TV ratio for each group. The highest value was displayed by ICA/CACB, followed by rhBMP-2/CACB, VAP/CACB, and pure CACB.

3.4.2. Histological assessment of newly formed bone
As shown in Fig. 6A, at 4 weeks post-implantation, the boundary between the defect area and the host bone tissue could still be clearly identified (marked by black arrows), with a similar histological characteristics observed in all groups. H-E staining showed fibrous connective tissue around the residual implanted scaffolds (Fig. 6A, b–e). Masson staining revealed that the fibrous tissue was mainly composed of newly formed collagen fibers (Fig. 6A, g–j). In the untreated group, fat vacuoles were observed to fill the defect area (Fig. 6A, a, f). At 12 weeks post-implantation, the interface between nascent bone and the host bone was indistinguishable in all treatment groups (Fig. 6B, b–e). ICA/CACB implantation resulted in the formation of normal and regular bony trabeculae and a mature bone marrow cavity (Fig. 6B, c, h). Although the defects were filled with new cancellous bone in the VAP/CACB and rhBMP-2/CACB groups, less trabecular and less mature bone marrow cavity was observed inside the defect area (Fig. 6B, d–e, i–j). Implantation of pure CACB without bioactive factors resulted in the least mature bone marrow cavity (Fig. 6B, b, g). The untreated defects were filled with fibrous tissue (Fig. 6B, a, f).

Fig. 2. Cumulative release [%] profiles of ICA (■), VAP (▲) and rhBMP-2 (●) from the corresponding ICA/CACB, VAP/CACB and rhBMP-2/CACB composites.

Fig. 3. In vitro bioactivity of rBMSCs on bioactive factor-loaded CACBs. (A) Scanning electron microscopy (SEM) images of rBMSCs seeded on (a) CACB, (b) ICA/CACB, (c) VAP/CACB, and (d) rhBMP-2/CACB after 24 h of culture. (B) The measured cell spreading areas. (C) Proliferation of rBMSCs grown on various scaffolds by CCK-8 assay. (D) Alkaline phosphatase (ALP) activity of rBMSCs cultured on various scaffolds at 4 and 10 days. (E) Gene expression of runt-related transcription factor-2 (RUNX-2), alkaline phosphatase (ALP), collagen 1α1 (COL1A1) and osteocalcin (OCN) in rBMSCs cultured on scaffolds.

### 3.4.3. COL I and OCN production in bone defects

COL I, a non-specific marker of osteogenesis, was strongly expressed within all treatment groups at both 4 and 12 weeks post-implantation (Fig. 7). Notably, the most intense positive staining was observed in the ICA/CACB group (Fig. 7A, c, h). The mRNA transcript levels of COL 1A1 (Fig. 7D-a) corresponded to the protein expression levels of COL I (Fig. 7C-a).

OCN, as a specific marker of bone maturation, was prevalent within the defects of all the implantation groups (Fig. 7B). The most intense staining was observed in the ICA/CACB group (Fig. 7B, c, h). The mRNA expression level of OCN (Fig. 7D-b) corresponded to OCN protein production (Fig. 7C-b).

3.4.4. Neovascularization capacity of scaffold composites in bone defects

Immunostaining of CD31 as a marker of newly formed blood vessels is shown in Fig. 8. At 4 weeks post-implantation, infiltrating blood vessels from the surrounding bone tissue were found at the periphery of the scaffold implants in all treatment groups (Fig. 8A, b–e). The calculated numbers of vascular sections for all CACB groups loaded with bioactive factors exhibited no significant difference, but were significantly higher than that of the pure CACB group without growth factors (Fig. 8B). At 12 weeks post-implantation, the ICA/CACB group exhibited the greatest number of capillary vessels (Fig. 8A-h, B). There were however no differences between the VAP/CACB and rhBMP-2/CACB groups (Fig. 8B). Pure CACB without bioactive factors displayed more vascular sections than the blank control. As shown in Fig. 8C, upon comparison with the CACB group, the mRNA levels of VEGF was dramatically up-regulated 5.36 ± 0.64 folds, 3.54 ± 0.38 folds and 3.73 ± 1.16 folds in the ICA/CACB, VAP/CACB and rhBMP-2/CACB groups respectively at 4 weeks post-implantation. Thereafter, the up-regulated VEGF expression levels decreased to 2.91 ± 0.87 folds, 1.20 ± 0.27 folds and 1.52 ± 0.55 folds in the ICA/CACB, VAP/CACB and rhBMP-2/CACB groups respectively at 12 weeks post-implantation.
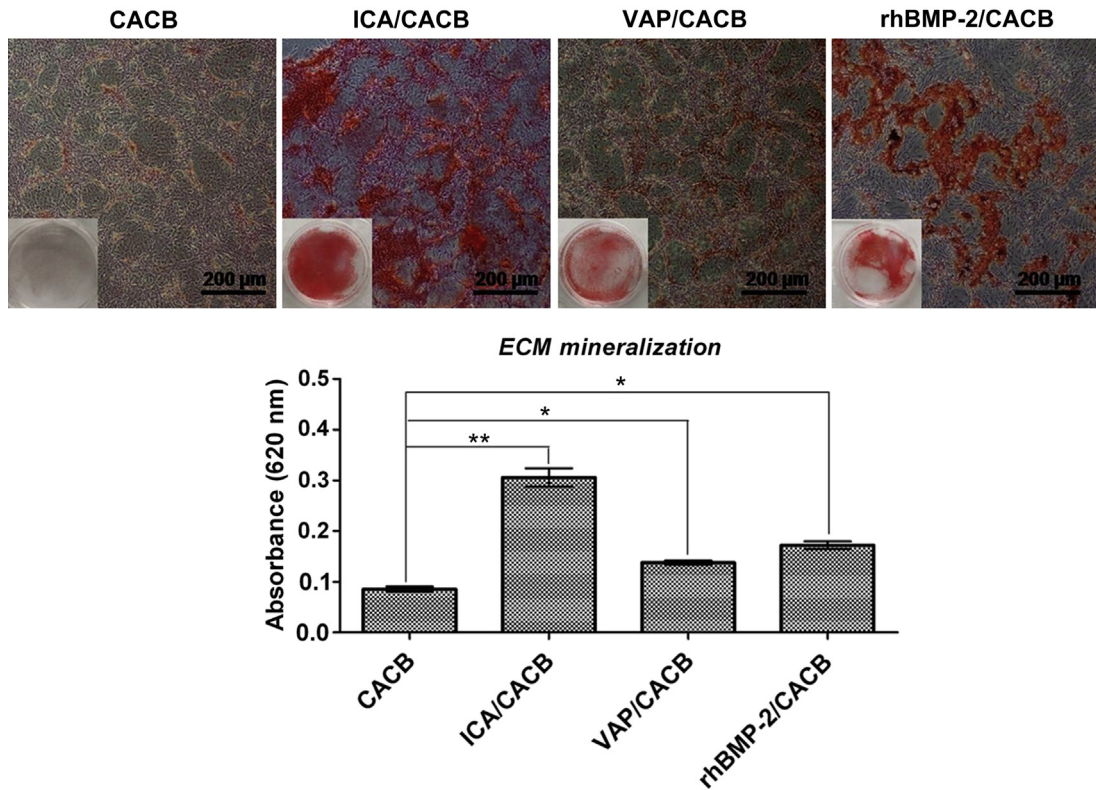
Fig. 4. Alizarin Red S staining and quantitative colorimetric results of rBMSCs cultured for 21 days in conditioned medium harvested from scaffold composites (100×). Insets show macroscopic images. Values represent the mean ± SD (*$p < 0.05$, **$p < 0.01$).
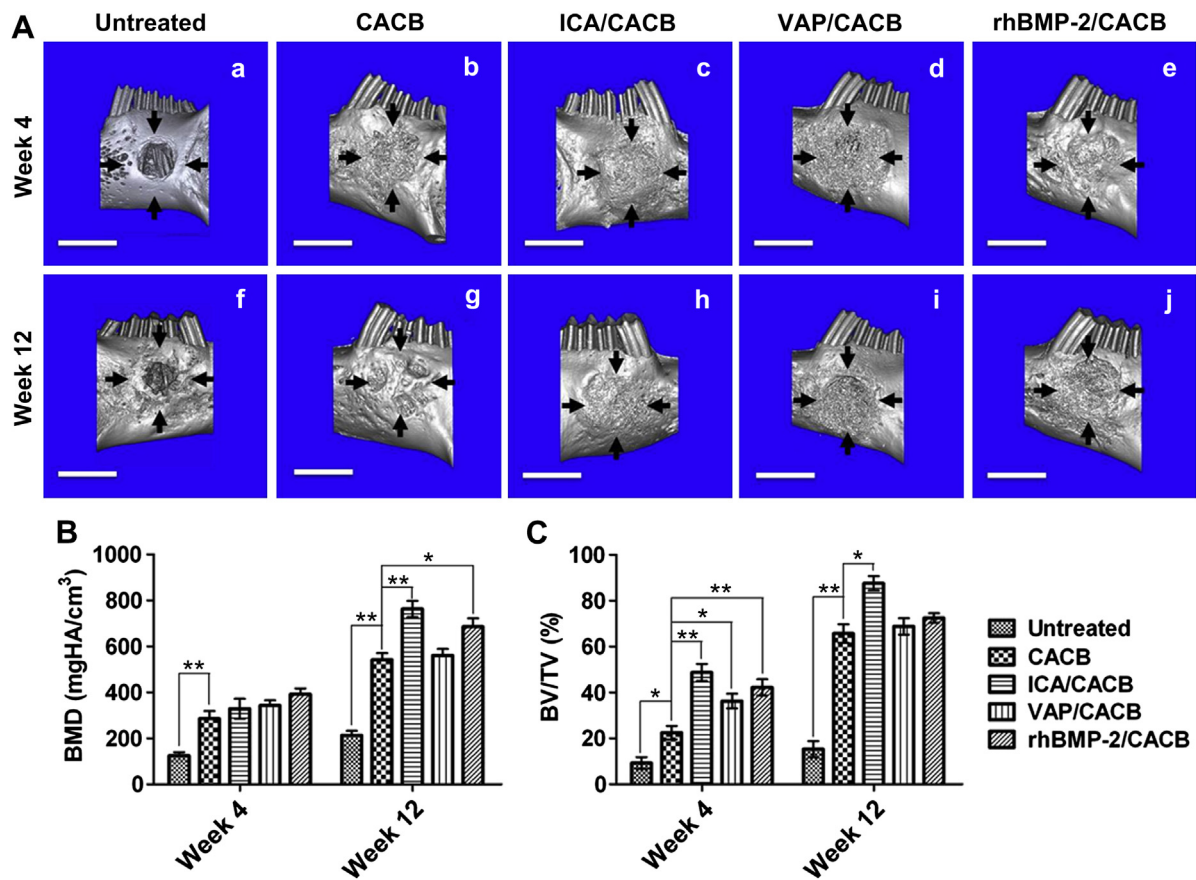
Fig. 5. Representative 3D μ-CT images of rabbit mandibular bone defects (A) and quantitative analysis of bone mineral density (BMD) (B) and the ratio of the bone volume/total volume (BV/TV ratio) (C) at 4 and 12 weeks post-implantation. Note that the image of 5A (f) for one of the untreated group is reproduced with permission from Fig. 5C of our previous study [32]. Scale bar: 8 mm. Black arrows denote the surgical site. (*$p < 0.05$ and **$p < 0.01$).
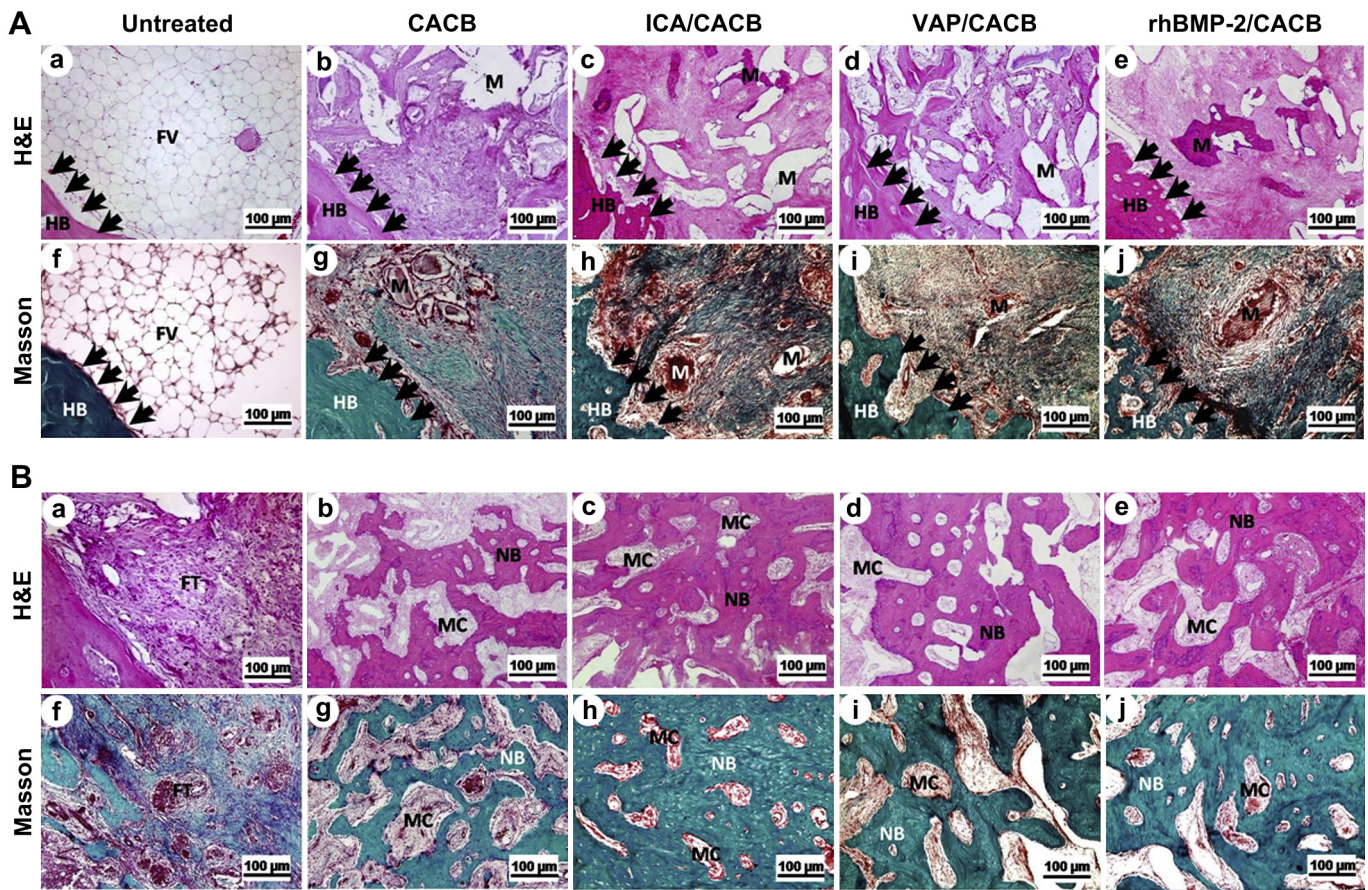
Fig. 6. Histological analysis of bone formation at (A) 4 weeks and (B) 12 weeks after implantation. (a–e) H&E staining; (f–j) Masson's trichrome staining; (a, f) untreated; (b, g) pure CACB; (c, h) ICA/CACB; (d, i) VAP/CACB; (e, j) rhBMP-2/CACB composites. Black arrows denote the boundary between nascent bone and host bone. (M: material; HB: host bone; NB: nascent bone; MC: medullary cavity; FV: fat vacuoles; FT: fibrous tissue).

3.4.5. Analyses of inflammatory gene expression

The mRNA transcript levels of pro-inflammatory (TNF-α, IL-6) and anti-inflammatory (IL-10) cytokines are shown in Fig. 9. ICA/CACB implants displayed the most reduced expression of TNF-α and IL-6. The differences between the pure CACB, VAP/CACB, and rhBMP-2/CACB groups were not significant, but the expression levels were significantly decreased compared to the blank control at both 4 and 12 weeks post-implantation. On the other hand, IL-10 mRNA levels at the ICA/CACB implantation site were significantly increased compared to the other experimental groups. The differences in IL-10 expression between the pure CACB, VAP/CACB, and rhBMP-2/CACB groups were not significant, but the expression levels were significantly increased compared to the blank control at both 4 and 12 weeks post-implantation. The agarose gel electrophoresis of PCR products displayed a similar trend as the quantitative data.

4. Discussion

To mimic the process of bone healing through action of autograft implantation, joint application of bioactive factors and CaP matrix scaffolds is of primary interest in bone defect repair. Proper interactions and synergistic performance between the loaded bioactive molecules and matrix scaffolds will lead to a favorable release of the appropriate dosage for the required time duration, and achieve optimal bone regeneration. So it is imperative and fundamental to understand the compatibility between bioactive factors and the scaffold matrix which might play pivotal role in determining the clinic outcomes of bone defect repair [41].

Calcinated antler cancellous bone (CACB) exhibited close similarity in its chemical composition and porous structure to those of human bone and displayed great potential for utilization in bone defect repair [32]. It can be reasonably inferred that CACB, once considered "bio-waste" in the past, might offer an alternative bone graft material that might overcome some of the disadvantages of other xenogenic grafts derived from bovine and porcine, such as time-consuming manufacturing process and especially controversial ethical issues pertaining to animal welfare [42–44]. SEM and μ-CT examinations demonstrated the porous and interconnected structure of CACB, with micropores existing within the walls of macropores. This architectural structure could facilitate bioactive factor loading and controlled release [45,46]. In this study, we used CACB as CaP based scaffolds owing to its reproducibility and easy accessibility, to evaluate the compatibility between CACB and various bioactive factors ICA, VAP, and rhBMP-2 which were derived from different species and compared their osteogenic performances both in vitro and in vivo.

In this study, tiny particulates of three bioactive factors loaded onto CACB scaffolds by physical adsorption were observed uniformly distributed on the surface of CACB scaffolds. Their presence and chemical stability was further confirmed by FT-IR spectra. However, there were obvious differences in their release profiles in vitro, which may be due to the inherent properties of these bioactive factors and their delicate interactions with CACB. ICA is a small molecule compound. The capillary force exerted by micro-
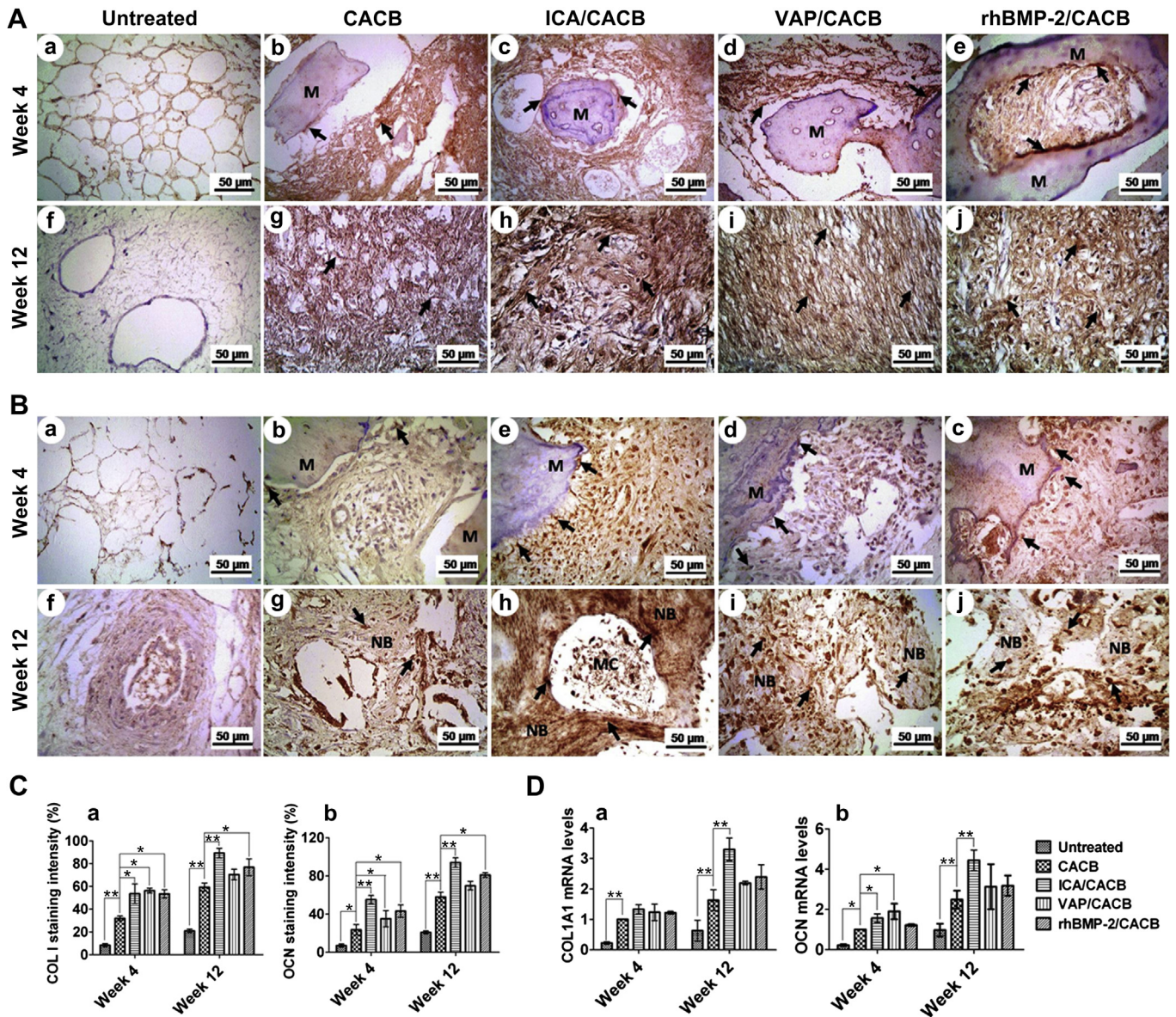
Fig. 7. COL I and OCN production in rabbit mandibular bone defects. (A) Immunohistological staining of COL I. (B) Immunohistological staining of OCN. (C) Staining intensity of COL I (a) and OCN (b). (D) mRNA transcription levels of COL 1A1 (a) and OCN (b). Values represent the mean ± SD ($n = 3$, $*p < 0.05$, $**p < 0.01$). The arrows denote the positive expression of COL I and OCN.

porosity such as the micropores on the wall of macropores of CACB might be the main reason for its strong diffusion capacity to penetrate the innermost part of the CACB scaffolds. This could result in relatively stable release of ICA from the ICA/CACB composites. The *in vitro* release results showed the largest burst release and almost all VAP released in VAP/CACB group, whereas minimal rhBMP-2 release was presented in rhBMP-2/CACB group during the entire assay duration. These results could be ascribed to the surface interactions between CaP matrix scaffolds and bioactive factors. Electrostatic interaction plays dominant role in the loading of protein bioactive factors onto apatite scaffolds through physical adsorption [47,48]. In the aspect of isoelectric point, there is a inherent difference between VAP and rhBMP-2, which is 4.5 [49] and 9.16 [50], respectively. When dissolved in PBS buffered at pH 7.4 at 37 °C (thereby mimicking physiological conditions), VAP has a nett negative surface charge, whereas rhBMP-2 exhibits a nett positive charge. On account of the negatively charged surface of

CACB in PBS, there were strong repulsive forces between VAP and the CACB scaffold surface, resulting in low affinity of CACB for VAP. In contrast, the attractive electrostatic interaction between rhBMP-2 and CACB scaffolds would result in stronger adsorption, consequently hindering the release of rhBMP-2 through simple diffusion. During the entire assay duration, not more than 20% of the adsorbed BMP-2 was released, which is consistent with the results reported by Chen et al. [35]. These results imply that it is necessary to take into account the physico-chemical properties and their possible interactions of target bioactive factors and CaP scaffolds when they are considered in combination for bone defect repair.

ICA is the main active component of *Epimedium*-derived flavonoids [7]. The dose-dependent effect of ICA on the proliferation and osteogenic differentiation of osteoblast cells has been studied extensively. There were reports that ICA concentrations ranging from 1×10^{-9} to 1×10^{-6} M had no cytotoxic effects toward human BMSCs [33] and MC3T3-E1 cells [51], whereas ICA above a
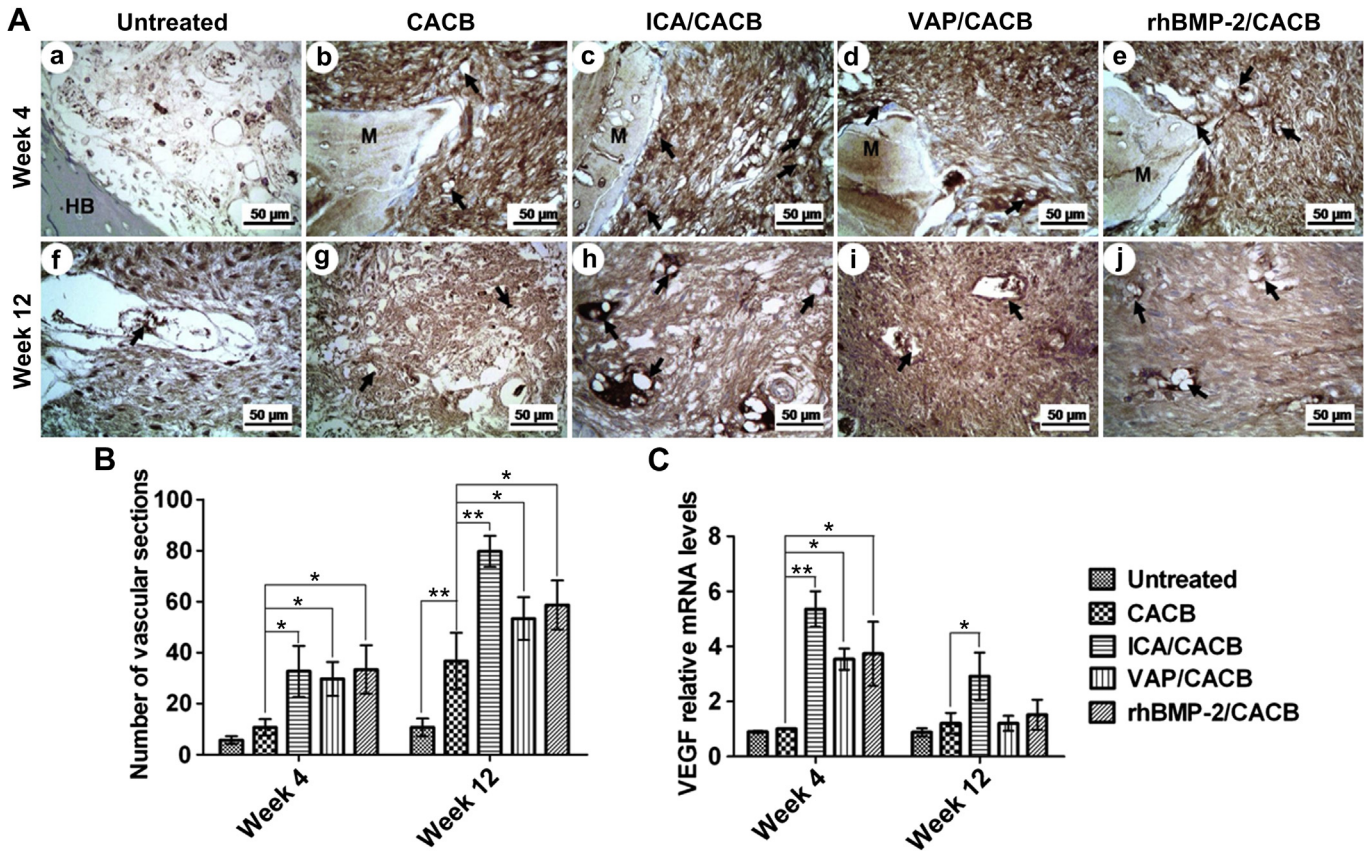
Fig. 8. Immunohistological staining of CD 31 after scaffolds implantation (A), quantitative analysis of the area of vascular sections (B) and mRNA transcript levels of VEGF (C). The arrows denote the newly formed blood vessels; Values represent mean ± SD ($n = 3$, $^*p < 0.05$, $^{**}p < 0.01$).

concentration of 10^{-5} M had high cytotoxicity. In our study, the cumulative amount of ICA released from the ICA/CACB scaffolds during the entire experimental duration was still less than 10^{-5} M, despite an initial burst release of ICA during the first 24 h. Previous studies have demonstrated that ICA is able to increase ALP activity, RUNX-2 and BMP-2 expression in primary osteoblasts [51,52]. Similarly, ICA/CACB scaffolds yielded enhanced ALP, RUNX-2, COL1A1 and OCN expression compared to CACB scaffolds alone in
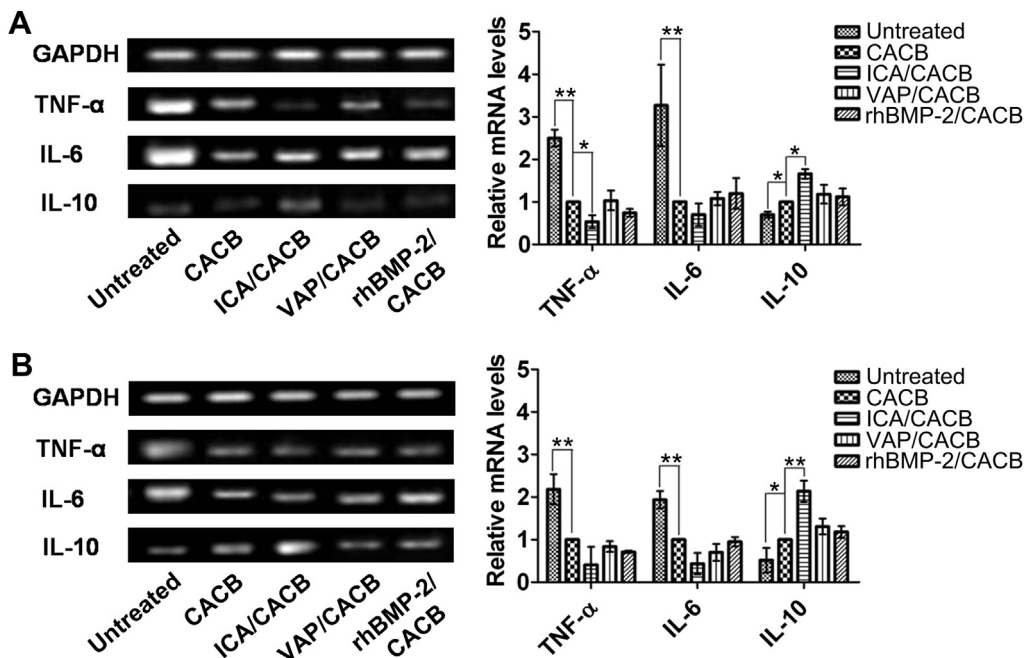
Fig. 9. Gel panel of the RT-PCR products and the mRNA expression levels of inflammatory genes at bone defect sites post-implantation for 4 weeks (A) and 12 weeks (B). Ratios of target genes relative to GAPDH were expressed as a percentage of the CACB group, which were set to 1. Values represent the mean ± SD ($n = 3$, $^*p < 0.05$, $^{**}p < 0.01$).

this study. The loading efficiency and relatively fast and stable release profile of ICA might contribute to its effects on the growth and osteogenic function of rBMSCs. VAP is polypeptide extracted from velvet antler [19]. There are reports that VAP could increase the proliferation and viability of osteoblast cells [53]. Similarly, in this study, the extended cell spreading area as well as increased cell proliferation was shown on VAP/CACB scaffolds. But ALP activity, mineralization, and mRNA transcript levels of osteogenic genes in VAP/CACB group were only mildly increased when compared to the CACB scaffolds alone. These results may be explained by the most rapid burst release of VAP from CACB. Moreover, this result was in agreement with previous report that VAP had no effect on ALP and OCN production by human alveolar osteoblasts [20]. BMP-2 has a pivotal role in regulating osteogenic differentiation [54]. In present study, the relatively low proliferation and osteogenic capacity of rBMSCs were shown on the rhBMP-2/CACB composite. This result could be ascribed to the extremely low release ratio of rhBMP-2 from the CACB scaffolds *in vitro*. Hence, on account of the compatibility and delicate interactions between bioactive factors and matrix scaffolds, there might be uncertainty in the bioactivity and bio-utility of the loaded bioactive factors. It is of prime importance to take into account their compatibility in considering their joint application in tissue regeneration, particularly when bioactive macromolecules are to be loaded on CaP ceramic scaffolds.

The *in vivo* osteogenic capacity of the experimental composites in critical-sized bone defect repair was further investigated. The results of μ-CT scanning, histological examination, immunohisto-chemical staining and mRNA transcript analysis showed that the ICA/CACB implant area possessed higher quality and quantity in bone formation and maturation when compared to VAP/CACB and rhBMP-2/CACB groups. These results confirmed that ICA had good compatibility with CACB in osteogenic ability. The result of neo-vascularization evaluation showed that the ICA/CACB group exhibited the greatest number of capillary vessels and highest VEGF gene expression level, which suggesting ICA possessed favorable neovascularization as reported by previous study that ICA could directly stimulate angiogenesis [55]. There is concensus that vascularization is a prerequisite for complete bone regeneration [56]. The reason of relatively better outcomes of VAP/CACB implant than CACB alone might be due to the multiple pleiotropic effects of VAP. In addition to stimulating osteoblast proliferation, VAP has been reported to promote chondrocyte proliferation and differen-tiation [59], which may enhance COL I and OCN production and facilitate callus formation [16]. Biodegradation *in vivo* should also be considered in explaining the osteogenesis differences observed amongst the active ingredients loaded scaffold groups. ICA is a phytomolecule with small molecular weight and relative stable structure. It is therefore unlikely to be degraded and should maintain bioactivity *in vivo* for a long time [57]. rhBMP-2, as a protein molecule with tertiary structure, easily denatures and loses its original bioactivity *in vivo* [35]. This degradation might also help to explain the relatively low osteogenic capacity of rhBMP-2/CACB observed in this study.

Interestingly, the production of anti-inflammatory cytokines was showed in positive correlation with the quantity of new bone formation while pro-inflammatory cytokines was in negative cor-relation among all experiment groups. From the immunological perspective, regulation of the immune reaction plays an important role in bone regeneration [58]. In the initial stages of bone repair with materials filling, moderate production of anti-inflammatory cytokines has been shown to be beneficial to bone formation [59] and the suppression of fibrosis [60]. In the untreated group, the defects areas were dominated by fibroblasts and adipocytes with excess pro-inflammatory cytokine production leading to fibrous

tissue formation [61,62]. The anti-inflammatory response concomitant with bone formation and neovascularization in our study indicates the importance of immune modulation in bone regeneration. The route from immune regulation to bone formation in bone defect repair is still unclear and requires further investigations.

5. Conclusions

In this study, the compatibility of CACB scaffolds with loaded ICA, VAP, or rhBMP-2, as well as their effects on the osteogenic potential of these composite scaffolds were investigated and compared *in vitro* and *in vivo*. A relatively stable release of ICA, a burst release of VAP, and only minimal release of rhBMP-2 from the corresponding composites were observed over a 14-day period *in vitro*. Among these composites, ICA/CACB composites displayed the most marked positive effects on rBMSC attachment, prolifera-tion, osteogenic differentiation and mineralization. The quality and quantity of *in vivo* bone formation and neovascularization with the ICA/CACB implant were superior compared to those of the VAP/CACB and rhBMP-2/CACB composites. The coincidence of an anti-inflammatory response with the observed outcomes of bone for-mation implied that the immune modulation mediated by bio-materials might play a pivotal role in the process of bone regeneration. These results thus highlighted the importance of compatibility between bioactive factors and matrix scaffolds in bone regeneration.

Acknowledgments

References

[1] Parikh SN. Bone graft substitutes in modern orthopedics. Orthopedics 2002;25:1301–9.
[2] Perka C, Schultz O, Spitzer RS, Lindenhayn K, Burmester GR, Sittinger M. Segmental bone repair by tissue-engineered periosteal cell transplants with bioresorbable fleece and fibrin scaffolds in rabbits. Biomaterials 2000;21:1145–53.
[3] Mehta M, Schmidt-Bleek K, Duda GN, Mooney DJ. Biomaterial delivery of morphogens to mimic the natural healing cascade in bone. Adv Drug Deliv Rev 2012;64:1257–76.
[4] Benders KE, Weeren PR, Badylak SF, Saris DB, Dhert WJ, Malda J. Extracellular matrix scaffolds for cartilage and bone regeneration. Trends Biotechnol 2013;31:169–76.
[5] Byers BA, Guldberg RE, Garcia AJ. Synergy between genetic and tissue engi-neering: Runx2 overexpression and in vitro construct development enhance in vivo mineralization. Tissue Eng 2004;10:1757–66.
[6] Yamamoto M, Tabata Y, Hong L, Miyamoto S, Hashimoto N, Ikada Y. Bone regeneration by transforming growth factor beta1 released from a biode-gradable hydrogel. J Control Release 2000;64:133–42.
[7] Zhao J, Ohba S, Komiyama Y, Shinkai M, Chung UI, Nagamune T. Icariin: a potential osteoinductive compound for bone tissue engineering. Tissue Eng Part A 2010;16:233–43.
[8] Richardson TP, Peters MC, Ennett AB, Mooney DJ. Polymeric system for dual growth factor delivery. Nat Biotechnol 2001;19:1029–34.
[9] Luginbuehl V, Meinel L, Merkle HP, Gander B. Localized delivery of growth factors for bone repair. Eur J Pharm Biopharm 2004;58:197–208.
[10] Matsumoto T, Okazaki M, Inoue M, Yamaguchi S, Kusunose T, Toyonaga T, et al. Hydroxyapatite particles as a controlled release carrier of protein. Bio-materials 2004;25:3807–12.
[11] Hu J, Hou Y, Park H, Lee M. Beta-tricalcium phosphate particles as a controlled release carrier of osteogenic proteins for bone tissue engineering. J Biomed Mater Res A 2012;100:1680–6.

[12] Liu T, Wu G, Wismeijer D, Gu Z, Liu Y. Deproteinized bovine bone functionalized with the slow delivery of BMP-2 for the repair of critical-sized bone defects in sheep. Bone 2013;56:110–8.

[13] King WJ, Krebsbach PH. Growth factor delivery: how surface interactions modulate release in vitro and in vivo. Adv Drug Deliv Rev 2012;64:1239–56.

[14] Varkey M, Gittens SA, Uludag H. Growth factor delivery for bone tissue repair: an update. Expert Opin Drug Deliv 2004;1:19–36.

[15] Shen W, Chen X, Chen J, Yin Z, Heng BC, Chen W, et al. The effect of incorporation of exogenous stromal cell-derived factor-1 alpha within a knitted silk-collagen sponge scaffold on tendon regeneration. Biomaterials 2010;31:7239–49.

[16] Street J, Bao M, deGuzman L, Bunting S, Peale Jr FV, Ferrara N, et al. Vascular endothelial growth factor stimulates bone repair by promoting angiogenesis and bone turnover. Proc Natl Acad Sci U S A 2002;99:9656–61.

[17] Urist MR. Bone: formation by autoinduction. Science 1965;150:893–9.

[18] Kang Y, Kim S, Khademhosseini A, Yang Y. Creation of bony microenvironment with CaP and cell-derived ECM to enhance human bone-marrow MSC behavior and delivery of BMP-2. Biomaterials 2011;32:6119–30.

[19] Guan SW, Duan LX, Li YY, Wang BX, Zhou QL. A novel polypeptide from Cervus nippon Temminck proliferation of epidermal cells and NIH3T3 cell line. Acta Biochim Pol 2006;53:395–7.

[20] Laky ZQ M, Ho E, Ulm C, Matejka M, Rausch-Fan X. The effect of deer antler growth factor on the viability and proliferation of primary human alveolar osteoblast cells in vitro. J Stomatol Occlusion Med 2009;2:175–8.

[21] Zhou QL, Guo YJ, Wang LJ, Wang Y, Liu YQ, Wang BX. Velvet antler polypeptides promoted proliferation of chondrocytes and osteoblast precursors and fracture healing. Acta Pharmacol Sin 1999;20:279–82.

[22] Ma HP, Ming LG, Ge BF, Zhai YK, Song P, Xian CJ, et al. Icariin is more potent than genistein in promoting osteoblast differentiation and mineralization in vitro. J Cell Biochem 2011;112:916–23.

[23] Chen KM, Ge BF, Ma HP, Liu XY, Bai MH, Wang Y. Icariin, a flavonoid from the herb Epimedium enhances the osteogenic differentiation of rat primary bone marrow stromal cells. Pharmazie 2005;60:939–42.

[24] Zheng D, Peng S, Yang SH, Shao ZW, Yang C, Feng Y, et al. The beneficial effect of Icariin on bone is diminished in osteoprotegerin-deficient mice. Bone 2012;51:85–92.

[25] Chen KM, Ge BF, Liu XY, Ma PH, Lu MB, Bai MH, et al. Icariin inhibits the osteoclast formation induced by RANKL and macrophage-colony stimulating factor in mouse bone marrow culture. Pharmazie 2007;62:388–91.

[26] Hsieh TP, Sheu SY, Sun JS, Chen MH. Icariin inhibits osteoclast differentiation and bone resorption by suppression of MAPKs/NF-kappaB regulated HIF-1alpha and PGE(2) synthesis. Phytomedicine 2011;18:176–85.

[27] Zhang X, Guo Y, Li DX, Wang R, Fan HS, Xiao YM, et al. The effect of loading icariin on biocompatibility and bioactivity of porous beta-TCP ceramic. J Mater Sci Mater Med 2011;22:371–9.

[28] Wang XL, Xie XH, Zhang G, Chen SH, Yao D, He K, et al. Exogenous phytoestrogenic molecule icaritin incorporated into a porous scaffold for enhancing bone defect repair. J Orthop Res 2013;31:164–72.

[29] Dorozhkin SV. Bioceramics of calcium orthophosphates. Biomaterials 2010;31:1465–85.

[30] El-Ghannam A. Bone reconstruction: from bioceramics to tissue engineering. Expert Rev Med Devices 2005;2:87–101.

[31] Tay BK, Patel VV, Bradford DS. Calcium sulfate- and calcium phosphate-based bone substitutes. Mimicry of the mineral phase of bone. Orthop Clin North Am 1999;30:615–23.

[32] Zhang X, Cai Q, Liu H, Heng BC, Peng H, Song Y, et al. Osteoconductive effectiveness of bone graft derived from antler cancellous bone: an experimental study in the rabbit mandible defect model. Int J Oral Maxillofac Surg 2012;41:1330–7.

[33] Fan JJ, Cao LG, Wu T, Wang DX, Jin D, Jiang S, et al. The dose-effect of icariin on the proliferation and osteogenic differentiation of human bone mesenchymal stem cells. Molecules 2011;16:10123–33.

[34] Bhakta G, Rai B, Lim ZX, Hui JH, Stein GS, van Wijnen AJ, et al. Hyaluronic acid-based hydrogels functionalized with heparin that support controlled release of bioactive BMP-2. Biomaterials 2012;33:6113–22.

[35] Chen SH, Wang XL, Xie XH, Zheng LZ, Yao D, Wang DP, et al. Comparative study of osteogenic potential of a composite scaffold incorporating either endogenous bone morphogenetic protein-2 or exogenous phytomolecule icaritin: an in vitro efficacy study. Acta Biomater 2012;8:3128–37.

[36] Zhao L, Liu L, Wu Z, Zhang Y, Chu PK. Effects of micropitted/nanotubular titania topographies on bone mesenchymal stem cell osteogenic differentiation. Biomaterials 2012;33:2629–41.

[37] Wang L, Fan H, Zhang ZY, Lou AJ, Pei GX, Jiang S, et al. Osteogenesis and angiogenesis of tissue-engineered bone constructed by prevascularized beta-tricalcium phosphate scaffold and mesenchymal stem cells. Biomaterials 2010;31:9452–61.

[38] Luo T, Wu C, Zhang Y. The in vivo osteogenesis of Mg or Zr-modified silicate-based bioceramic spheres. J Biomed Mater Res A 2012;100:2269–77.

[39] Tuominen VJ, Ruotoistenmaki S, Viitanen A, Jumppanen M, Isola J. ImmunoRatio: a publicly available web application for quantitative image analysis of estrogen receptor (ER), progesterone receptor (PR), and Ki-67. Breast Cancer Res 2010;12:R56.

[40] Livak KJ, Schmittgen TD. Analysis of relative gene expression data using real-time quantitative PCR and the 2(-Delta Delta C(T)) method. Methods 2001;25:402–8.

[41] Subramani K, Ahmed W. Emerging nanotechnologies in dentistry: processes, materials and applications. William Andrew; 2011.

[42] Amirfeyz R, Stanley D. Allograft-prosthesis composite reconstruction for the management of failed elbow replacement with massive structural bone loss: a medium-term follow-up. J Bone Jt Surg Br 2011;93:1382–8.

[43] Mellor DJ, Littin KE. Using science to support ethical decisions promoting humane livestock slaughter and vertebrate pest control. Anim Welfare 2004;13:127–32.

[44] Yang YG, Sykes M. Xenotransplantation: current status and a perspective on the future. Nat Rev Immunol 2007;7:519–31.

[45] Bose S, Tarafder S. Calcium phosphate ceramic systems in growth factor and drug delivery for bone tissue engineering: a review. Acta Biomater 2012;8:1401–21.

[46] Ginebra MP, Canal C, Espanol M, Pastorino D, Montufar EB. Calcium phosphate cements as drug delivery materials. Adv Drug Deliv Rev 2012;64:1090–110.

[47] Lee WH, Zavgorodniy AV, Loo CY, Rohanizadeh R. Synthesis and characterization of hydroxyapatite with different crystallinity: effects on protein adsorption and release. J Biomed Mater Res A 2012;100:1539–49.

[48] Gilbert M, Shaw WJ, Long JR, Nelson K, Drobny GP, Giachelli CM, et al. Chimeric peptides of statherin and osteopontin that bind hydroxyapatite and mediate cell adhesion. J Biol Chem 2000;275:16213–8.

[49] Guo Y, Ma M, Sun R, Chen L, Song Y, Deng XM. Biodegradable gelatin/beta-tricalcium phosphate composite microspheres as localized delivery of growth factor-velvet antler polypeptides by water-in-oil (W/O) emulsion process. 2009 ICBBE 2009 3rd International Conference on: IEEE; 2009. p. 1–4. Bioinformatics and Biomedical Engineering.

[50] Patterson J, Siew R, Herring SW, Lin AS, Guldberg R, Stayton PS. Hyaluronic acid hydrogels with controlled degradation properties for oriented bone regeneration. Biomaterials 2010;31:6772–81.

[51] Zhao J, Ohba S, Shinkai M, Chung UI, Nagamune T. Icariin induces osteogenic differentiation in vitro in a BMP- and Runx2-dependent manner. Biochem Biophys Res Commun 2008;369:444–8.

[52] Cao H, Ke Y, Zhang Y, Zhang CJ, Qian W, Zhang GL. Icariin stimulates MC3T3-E1 cell proliferation and differentiation through up-regulation of bone morphogenetic protein-2. Int J Mol Med 2012;29:435–9.

[53] Weng L, Zhou QL, Ikejima T, Wang BX. A new polypeptide promoting epidermal cells and chondrocytes proliferation from Cervus elaphus Linnaeus. Acta Pharmacol Sin 2001;36:913–6.

[54] Urist MR, Strates BS. Bone morphogenetic protein. J Dent Res 1971;50:1392–406.

[55] Xiao-Hong D, Chang-Qin X, Jian-Hua H, Wen-Jiang Z, Bing S. Icariin delays homocysteine-induced endothelial cellular senescence involving activation of the PI3K/AKT-eNOS signaling pathway. Pharm Biol 2013;51:433–40.

[56] Petite H, Viateau V, Bensaid W, Meunier A, de Pollak C, Bourguignon M, et al. Tissue-engineered bone regeneration. Nat Biotechnol 2000;18:959–63.

[57] Xie XH, Wang XL, Zhang G, He YX, Wang XH, Liu Z, et al. Structural and degradation characteristics of an innovative porous PLGA/TCP scaffold incorporated with bioactive molecular icaritin. Biomed Mater 2010;5:054109.

[58] Franz S, Rammelt S, Scharnweber D, Simon JC. Immune responses to implants - a review of the implications for the design of immunomodulatory biomaterials. Biomaterials 2011;32:6692–709.

[59] Ratanavaraporn J, Furuya H, Tabata Y. Local suppression of pro-inflammatory cytokines and the effects in BMP-2-induced bone regeneration. Biomaterials 2012;33:304–16.

[60] Kou PM, Babensee JE. Macrophage and dendritic cell phenotypic diversity in the context of biomaterials. J Biomed Mater Res A 2011;96:239–60.

[61] Kim SE, Song SH, Yun YP, Choi BJ, Kwon IK, Bae MS, et al. The effect of immobilization of heparin and bone morphogenic protein-2 (BMP-2) to titanium surfaces on inflammation and osteoblast function. Biomaterials 2011;32:366–73.

[62] Wu G, Liu Y, Iizuka T, Hunziker EB. The effect of a slow mode of BMP-2 delivery on the inflammatory response provoked by bone-defect-filling polymeric scaffolds. Biomaterials 2010;31:7485–93.